New generation of dual polarized weather radars in Austria

Rudolf Kaltenboeck

Austrocontrol - Aviation Weather Service, Vienna, Austria, rudolf.kaltenboeck@austrocontrol.at

(Dated: 30 May 2012)

1. Abstract

Austrocontrol as air service provider operates Austrian weather radar network for aeronautical meteorological purpose and is going to renew the full Austrian weather radar network to simultaneous transmitting dual polarized radars till 2013. The main goal of the Austrian radar exchange is the use of polarimetric and Doppler applications and the improvement of data quality including change of scan strategy. The new interleave scan strategy offers the possibility of long range volume scans with update intervals of 2.5 minutes. After the first dual pol weather radar installation in 2006 two new radars were installed close to Vienna (2010) and Salzburg (2011) respectively. The dual pol data in Austria will be used for nowcasting of severe weather for aviation purpose e.g., icing hazards, hail detection/quantification, to localize up/downdraft positions within convective systems, lighting forecasting and to interpret mesoscale features in more detail by analyzing new polarimetric moments. Additionally these data will be used to improve the data quality by discrimination between different precipitation types and nonmeteorological echoes and for QPE (quantitative precipitation estimations).

2. Motivation

Weather phenomena especially thunderstorms during summer may strongly affect safety and economic aspects of aviation. The influence of weather increases in dense air traffic network when strong coupling between terminal and en-route delays occur. Weather radars have the ability to identify significant convection by subscale phenomena in high time and spatial resolution. These data provide valuable 3D information for anticipation and nowcasting of thunderstorms.

Fig.1 shows Austrian composite of weather radar maximum projected reflectivity (>35 dBZ) overlaid by aircraft tracks (10 minutes history, latest position in red) from 17th July 2010 2015 UTC. Austrian border lines drawn in green, Austrian international airports are indicated as black triangle. Thunderstorms over central and eastern part of Austrian FIR and in the vicinity / over Vienna international airport (LOWW) strongly affect en-route and approach corridors, causing delays to all flights. Rerouting air ways and several holding patterns for approach to LOWW are shown.
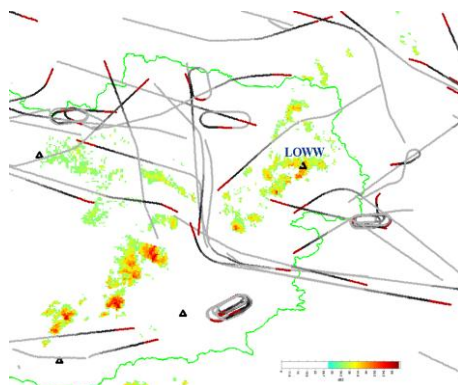

Fig.1 shows weather radar data overlaid by flight tracks over the eastern part of Austria. Thunderstorm activity results in rerouting and holding patterns.

3. Austrian weather radar network

Fig.2: Austrian weather radar network.

The operational weather radar network in Austria consists of 5 stations (Fig.2), where 2 stations are situated at lower altitudes close to international airports and others are mountain sites above altitudes of 2000 m msl. All weather radars (WXR) are manufactored by EEC and operate at C band (5600-5650 MHz). The new radar type is DWSR-5001C/SDP/CE (antenna pedestal mounted receiver) including 500 kW solid state modulator, Gamic Enigma III+ signal processor, 4.2 m sandwich antenna and AFC 6 m stealth radome with hydrophobic coating. Due to the 500 kW peak power, we expect no loss in sensitivity compared to our old radar system. The radars of Rauchenwarth (RAU) / Feldkrichen (FEL) are already renewed and operational since March / December 2011 respectively. Further 2 new radars will be installed in summer 2012 (Ziribitzkogel - ZIR) and 2013 (Patscherkofel - PAT) at Alpine mountain tops. The Valluga radar, in the western part of Austria is in operation since 2007 and has polarized capabilites, too. This older type of EEC Sidpol radar consists of antenna pedestal mounted EDRP9 signal processor, 250 kW peak power and orange peel radome.

4. Interleave scan strategy

Clever scanning strategies are needed to minimize the delay of radar images, when 10 minutes are equivalent to 120-140 km flight distance. Additional volume coverage is needed for aviation prupose such as e.g. icing hazards, hail aloft, lighting potential or turbulences. Interleave scan strategy (Fig.3) offers the possibility of high update rates accompanied by volume coverage (e.g. Joss et al., 1998) and applied on new installed Austrian radars.
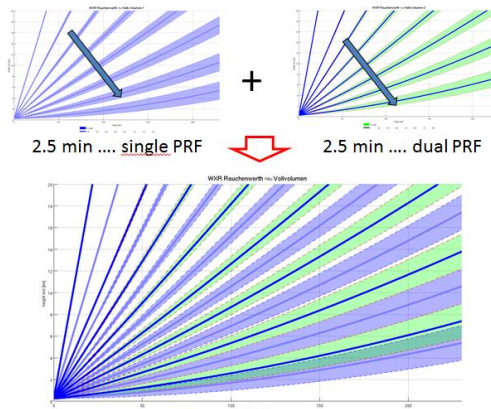

Fig.3: Interleave scan strategy. Full volume scan consists of two half scans of different elevations (3dB beam width is colored in blue/green for half scan 1/2).

Each half scan consists of 8 elevations (approx. duration of 2.5 min) by applying variable antenna rotation speeds (Tab.1). The latest two half scans are combined and updated every 2.5 min. Subsequent full volume scan covers 16 elevations. For each half scan the scan sequence is from top to bottom with corresponding time stamp at lowest level (the latest sweep is the actual one and closest to the ground). High update rates are the advantage of this scan process. But fast moving and fast developing storms reveal discontinuities and displacements in cross sections analyses by using combination of two previous half scans.

To increase the Doppler velocity for nowcasting application, dual PRF sampling is applied on the second half scan. Due to the operation in STAR mode following moments are collected by Austrian radars: radar reflectivity (Z_H), Doppler velocity (V_H) and the polarimetric moments as differential reflectivity (Z_{DR}), copolar cross-correlation coefficient (ρ_{hv}) and differential phase (ϕ_{DP}). The operational use of linear depolarization ratio (LDR) is not planed yet. Vertical pointing Z_{DR} calibration scans are executed every 15 min. Elevation and range are selected to cover entire Austrian air space (FIR), overlapping to the next radar site as well as collecting volume coverage up to 10 km height to the closet international airport. Puls lengths and range bin resolution is 0.8 µs and 250 m respectively. Antenna beam width is 0.88 degree.

	Elevation	Range (Z)	rotation		PRF	vmax
	Grad	km	1/min	°/s	Hz	m/s
Interleave 1	33 (90)	100	6	36	1500	20
	18	100	6	36	1500	20
	12	125	6	36	1200	16
	8,3	125	6	36	1200	16
	5,6	186	4	24	800	11
	3,5	224	3	18	670	9
	1,8	224	3,3	20	600	8
	0,5	224	3	18	600	8
Interleave 2	65	100	6	36	800/1200	32
	22	100	6	36	800/1200	32
	14,5	100	6	36	800/1200	32
	10	125	6	36	800/1200	32
	6,8	186	4	24	600/800	32
	4,5	186	3,3	20	600/800	32
	2,6	224	3,3	20	480/600	32
	1	224	3	18	480/600	32

Tab.1: Scan strategy for WXR RAU (Rauchwarth).

4. Doppler products

Unfolded Doppler velocities can be well used for nowcasting and auotmaic diagnosis for aeronautical warnings like gust front identifcation and shear warnings. An example is given in Fig.4.
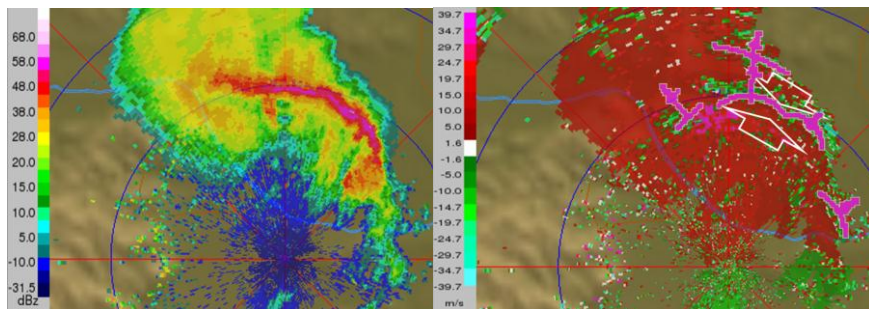

Fig 4: Bow echo in the vicinity of Vienna from 27ᵗʰ May 2011 1247 UTC. Z_H and V_H at PPI elevation 1° are shown. Doppler wind field is overlaid by gust front identifcation. White arrows indicate convergent Doppler wind pattern.

5. Raw PPIs for nowcasting

In the past, only products have been made available to operational Austrian forecasters, which have been post-processed and corrected before. Subscale features especially in reflectivity data might have been lost. In near future, raw data at PPI will be available to forecasters to use such mesoscale feature like convergence lines for gust front detection (Fig.5) and to anticipate wind changes and possible thunderstorm initiation (Wilson et al., 1998), see Fig.6. Nowcasting these features, PPI images may especially help in case of intensifying gust fronts or low coverage of surface observation. At lowlands in Austria, dry and wet cases of convergence zones frequently occur north and east of the Alps (e.g. Kaltenboeck, 2004).
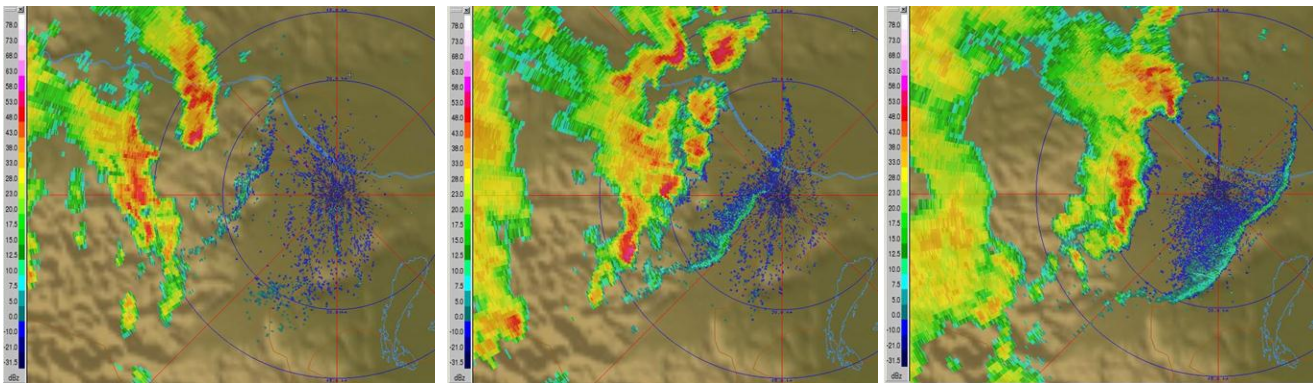
5.1. Convergence line – wind shift, dry case:

Fig.5: Z_H at PPI 1.8° from WXR RAU, 5ᵗʰ Sep. 2011 for 1300, 1330 and 1400 UTC. Convergence fine line of low reflectivity caused by thunderstorm outflow results in wind shift at Vienna international airport from 15020kt to 29021g31kt accompanied by drop in temperature of 12 K.
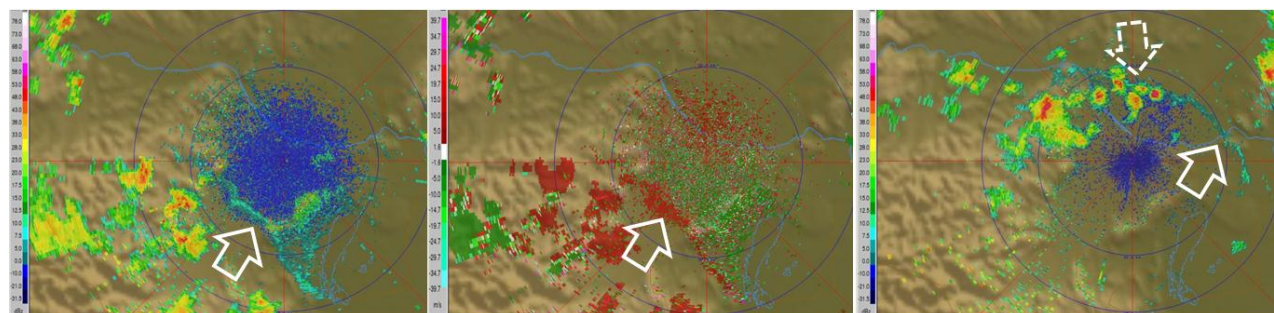
5.2. Convergence line – thunderstorm initiation:

Fig.6: Convergence line (marked by white arrows) as fine line in ZH (left) and Doppler velocity (middle panel) from 21ˢᵗ May 2011 1302 UTC at PPI elevation 1° WXR RAU. Triggering of thunderstorms along convergence line is marked by dashed arrow (1457 UTC). Wind at Vienna airport changed from 03008kt to 21013kt, which is relevant for runway in use.

6. Examples of polarimetric application

6.1. Convergence line

Convergence lines are marked as fine lines of low radar refelctivity (Fig.5, 6). Accompanied polarimetric signatures in Fig.7 are high values of Z_{DR} (up to 4 dB) and low values of ρ_{hv} (0.5) due to lifted insects and nonmeteorological targets.
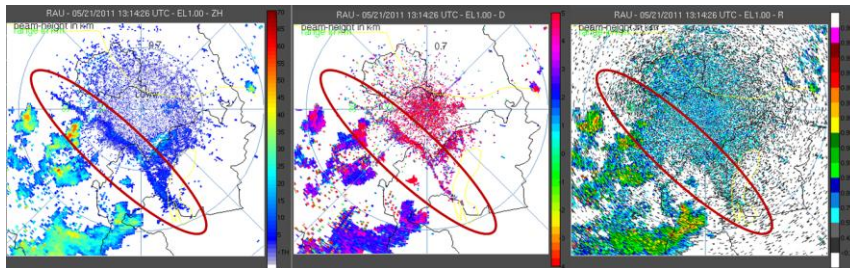

Fig.7: as Fig.6 but for polarimetric variables for 13:14UTC. From left to right: Z_H, Z_{DR}, and ρ_{hv}. Convergence zone is marked by red ellipse. Range ring distance is 25 km in left panel.

6.2. Polarimetric hail signature of large hail

Vertical polarimetric hail signature of large hail at C band (e.g. Kaltenboeck and Ryzhkov, 2012a) is shown in Fig.9+10 for nontornadic supercell which caused hail size of 3 cm in the area of Kirchstetten / NÖ and detected by WXR RAU. Fig.9 shows large Z_{DR} and low ρ_{hv} values due to resonant scatters and melting hail mixed with rain. Size sorting is manifested as Z_{DR} arc (> 4 dB) in the area of the rear flank downdraft. There, the part of the storm is facing toward the radar (compare with Kaltenboeck and Ryzhkov, 2012b). Note, corrections for attenuation, Z_{DR} bias, system ϕ_{DP} and ρ_{hv} have been applied (e.g. Kaltenboeck and Ryzhkov, 2012a). At the backside of the storm (with respect to the radar) differential attenuation (negative Z_{DR}, large ϕ_{DP}) can be seen.
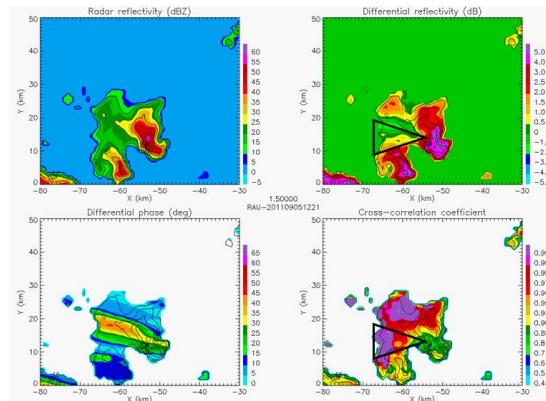

Fig.8: Polarimetric hail signature below freezing level seen by WXR RAU from 5th Sep. 2011 1221 UTC. CAPPI height is 1.5 km. Upper and lower panels show Z_H/Z_{DR} and ϕ_{DP}/ρ_{hv} respectively. Reported hail size diameter is 3 cm. Arrows indicate hail signature within cell core center accompanied by high values of Z_{DR} (>5 dB) and low values of ρ_{hv} (0.7).

Above freezing level in the wet growth regime, Z_{DR} and ρ_{hv} holes clearly indicate the presence of large hail (Fig.9) within areas of high values of Z_H.
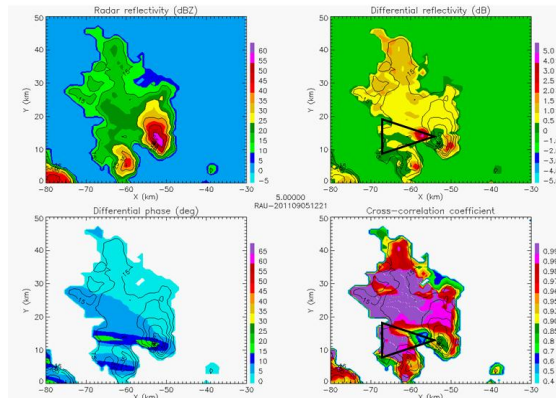

Fig.9: same as in Fig.8 except at 5 km CAPPI height (-10 °C wet bulb temperature height). Arrows mark well pronounced Z_{DR} hole (0 dB) and ρ_{hv} hole (0.85) above freezing level.

6.3. Updraft identification: Z_{DR} column

The cross section in Fig.10 shows Z_{DR} column (ZDR>2 dB) associated with updraft up to 6 km on the eastern flank of hail bearing cell over Pinkafeld / BGL from 2nd Sept. 2011 1740 UTC. The reported hail size is 5 cm. The Z_{DR} column develops when large raindrops are lifted above the freezing level.
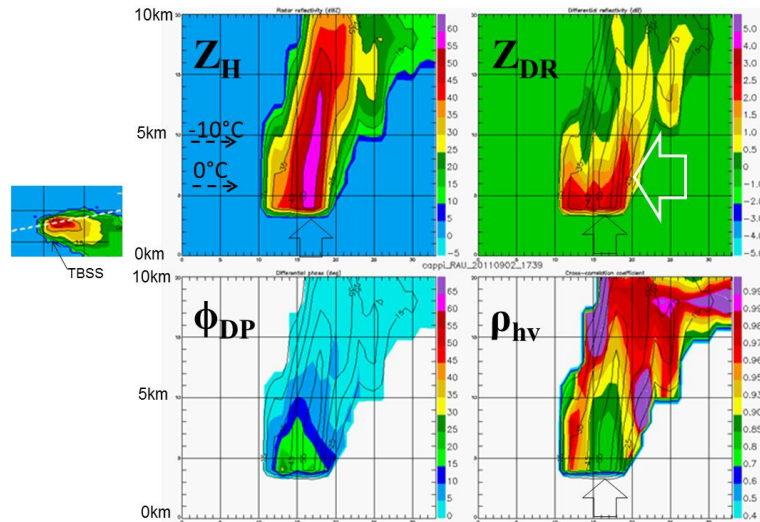

Fig.10: W-E cross section throw hail bearing cell from 2nd Sep. 2011 1740 UTC seen by WXR RAU. Z_{DR} column (marked by white arrow) identifies the updraft location. Polarimetric hail signature below freezing level is marked by black arrows (Z_{DR}>2dBZ, ρ_{hv}<0.8). Low values of ρ_{hv} aloft (at -10 °C height) indicate severe hail generation.

6.4 Snowfall events

A cold snow fall event is shown in Fig.11. Reported surface temperature is -11 °C accompanied by strong northwesterly winds. Anisotropic, not aggregated crystals result in low values of Z_H (5-15 dBZ) and high values of Z_{DR} (2-3 dBZ) (compare with e.g. Ryzhkov et al., 2008).
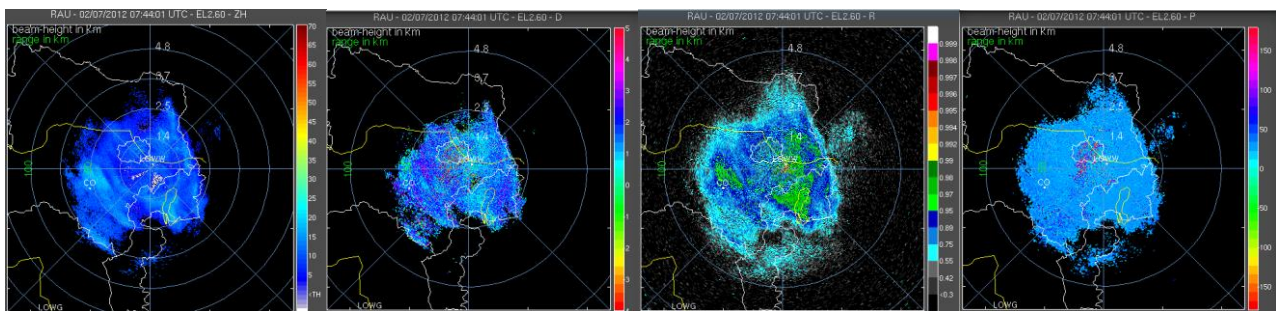

Fig. 11: PPI at 2.6° from WXR RAU, 7th Feb. 2012 0744 UTC. Z_H, Z_D, ρ_{hv} and ϕ_{DP} are shown from left. Range ring distance is 25 km in left panel.

In contrast, in the melting layer close to the surface (3 °C and rain was observed at Salzburg int. airport), Z_H values exceed 30 dBZ (close to the radar site) accompanied by decreased ρ_{hv} in Fig.12. Dry aggregated snow just above the bright band, reveal typical Z_{DR} values close to 0 dB. Especially at far northern ranges slightly negative Z_{DR} occur and might be caused by differential attenuation (compare to Saltikoff et al., 2010).
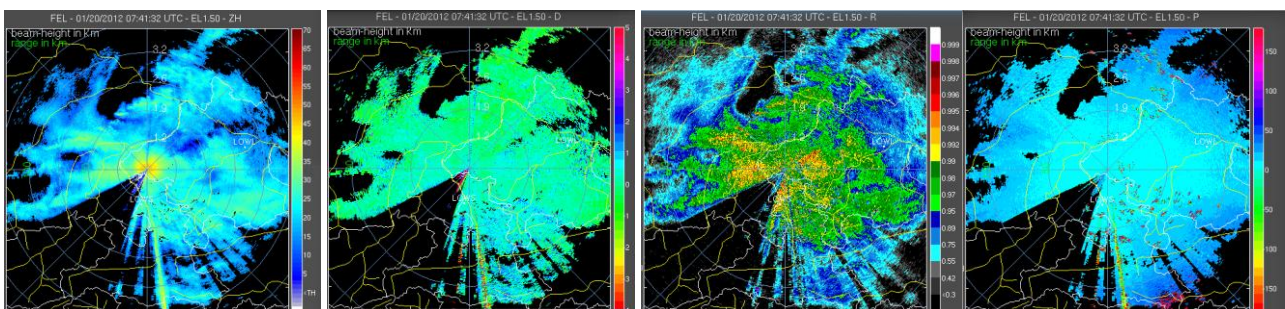

Fig.12: as Fig.11 except for elevation 1.5° from WXR FEL, 20th Jan 2012 0741UTC.

6.5. Bright band

Polarimetric melting layer identification helps to localize areas of hazardous icing. A pronounced bright band is indicated as enhanced circle of Z_H (up to 40 dBZ), Z_{DR} (up to 4 dB), decreased ρ_{hv} (< 0.75) and slightly increased ϕ_{DP} in Fig.13. It is embedded in stratiform rain from 18th June 2011 2358 UTC in the vicinity of Vienna. Z_{DR} shows positive values (around 2 dB) in rain (closer to the radar site) and lower values (around 0 dB) above the melting layer (radial outside of the Z_H circle).
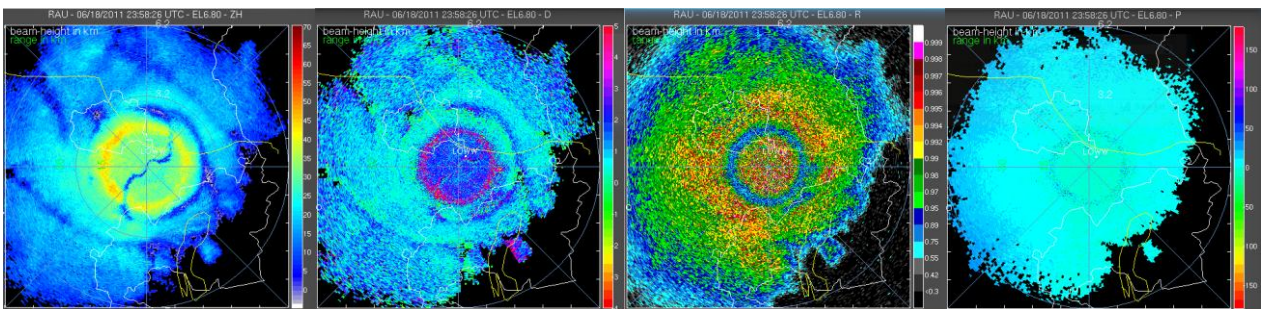

Fig.13: Bright band is embedded in stratiform rain in PPI image with elevation 6.8° from WXR RAU, 18th June 2011 2358 UTC. From left to right, panels show Z_H, Z_{DR}, ρ_{hv}, ϕ_{DP}. Range ring distance is 25 km in left panel.

6.5. Ground clutter

Polarimetric data (or texture) can be well used for the discrimination between meteorological and nonmeteorological echos such as ground clutter (e.g. Gourley et al., 2007). An example for decreasing of ρ_{hv} in areas which are contaminated by ground clutter is presented in Fig.13 for the eastern part of the Alps.
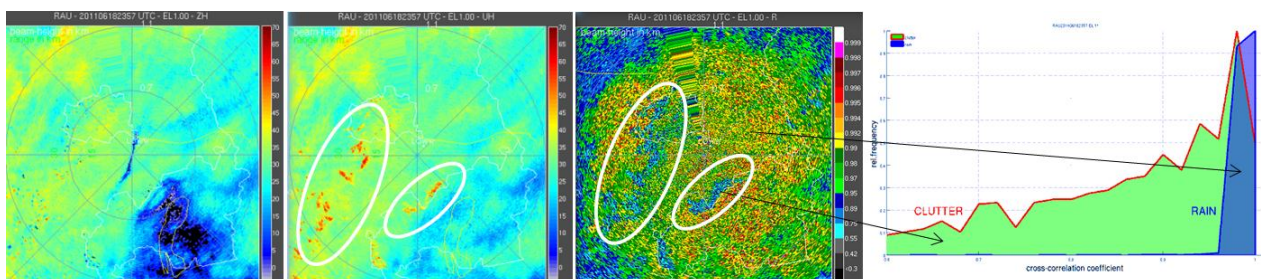

Fig.14: From left to right, panels show Z_H, U_H (unfiltered reflectivity) and ρ_{hv} at PPI images with elevation 1° from WXR RAU, 18th June 2011 2358 UTC. Ground clutter contaminated areas are marked in white. Outer range circle radius is 50 km. Statistical distribution of ρ_{hv} for ground clutter compared to stratiform rain is given in the right panel.

7. Conclusion and outlook

Collected data of dual polarized radars in Austria including new scan strategy have successfully demonstrated new applications in aviation weather service provision during past years test phase. Calibration and monitoring issues of polarimetric variables are quite important. Next steps in Austrocontrol weather radar exchange project will be: a) renewing of 2 further radars at mountain tops, b) extension of calibration and monitoring issues, c) integration of (dual-) Doppler and polarimetric products in our new operational visualization system, d) implementation of polarimetric methods for data quality assessment and e) verification and fine-tuning of hydro classification schema and QPE.

Acknowledgment

References

Gourley, J., Tabary, P., and Parent du Châtelet, J., 2007: A fuzzy logic algorithm for the separation of precipitating from nonprecipitating echoes using polarimetric radar observations. *J. Atmos. Oceanic Technol.*, **24**, 1439–1451.

Joss, J. et al, 1998: Operational Use of Radar for Precipitation Measurements in Switzerland. vdf Hochschulverlag AG an der ETH Zürich. ISBN 3-7281-2501-6, 108pp [available online at: http://www.meteoswiss.admin.ch/web/en/research/projects/rain.Related.0002.DownloadFile.tmp/onlinedocumentation.pdf]

Kaltenboeck, R., 2004. The outbreak of severe storms along convergence lines northeast of the Alps. Case study of the 3 August 2001 mesoscale convective system with a pronounced bow echo. *Atmos. Res.* **70**, 55–75.

Kaltenboeck, R. and Ryzhkov, A., 2012a: Comparison of polarimetric signatures of hail at S and C bands for different hail sizes. *Atmos. Res.,* accepted, doi: 10.1016/j.atmosres.2012.05.013

Kaltenboeck, R. and Ryzhkov, A., 2012b: Comparison of polarimetric radar signatures in hailstorms simultaneously observed by C-band and S-band radars. *Extended Abstracts*, 7th Europ. Conf. on Radar in Met. and Hydr., Toulouse, France

Ryzhkov, A. et al., 2008: Polarimetric characteristics of snow measured by radar and 2D video disdrometer. *Extended Abstracts*, 5th Europ. Conf. on Radar in Met. and Hydr., Helsinki, Finland

Saltikoff, E. et al., 2010: Negative ZDR in stratiform snow with C-band. *Extended Abstracts*, 6th Europ. Conf. on Radar in Met. and Hydr., Sibiu, Rumania

Wilson, J. et al., 1998. Nowcasting thunderstorms: a status report. *Bull. Am. Meteorol. Soc.,* **79**, 2079–2099.